Energy & Environmental Science

REVIEW

View Article Online
View Journal | View Issue

Cite this: *Energy Environ. Sci.*, 2015, **8**, 824

Received 22nd October 2014
Accepted 7th January 2015

DOI: 10.1039/c4ee03346a

www.rsc.org/ees

Light management in thin film silicon solar cells

F.-J. Haug* and C. Ballif

Thin film silicon is an attractive and versatile material for photovoltaics whose manufacturing reached a high level of maturity. Owing to its moderate efficiency compared to crystalline technologies, it should target either power plants with low installation cost or applications with added value like building-integration. Since the technology relies on very thin films of a weakly absorbing material, light-management is, and always has been, a key aspect of the technology. In this review, we briefly describe the class of materials that is summed up under the name "thin film silicon", point out requirements on device design, and discuss functionalities that enhance the absorption in the silicon films, addressing both their theoretical understanding as well as experimental realization.

Broader context

Thin film silicon is a mature and reliable photovoltaic technology. Combined with tin- or zinc-based transparent contacts, it is based entirely on earth-abundant materials and the resulting modules have a low energy-payback time. The products are aesthetically pleasing and well suited for building integration. This review gives a brief summary on the historical development of the material, its manufacturing processes and optical properties, and it discusses requirements for cell-design. The remainder of the article is devoted to a discussion of the ongoing efforts to capture a maximum of the incident light and to convert it with a minimum of parasitic losses. Here, thin film silicon has often served as a test-bed for novel concepts and the ensuing results can thus provide valuable insight for other technologies.

Introduction

Ever since photovoltaics was considered seriously as a means for power generation, *i.e.* since the mid 50s of the last century, concerns about the cost of crystalline silicon substrates inspired research in alternatives based on thin films. After the rise and fall of the CuS/CdS technology, research on CdTe started in the late 60s, followed by $CuInSe_2$ in 1975. Amorphous silicon entered the scene in 1976 with the demonstration of n- and p-type doping by Spear and Le Comber[1] and the first amorphous silicon solar cell by Carlson and Wronski.[2] Thin film silicon is thus the youngest of "old" thin film technologies.

Different from its crystalline counterpart, amorphous silicon does not suffer from the weak absorption of an indirect bandgap,[3,4] but the characteristic of its absorption coefficient is still closer to the square-law of indirect semiconductors than to the square-root of direct ones. Thus, light with energy close to the bandgap is absorbed only weakly and makes absorption enhancement a necessity. There is a second motivation because relatively poor electronic transport in the amorphous material requires a device design based on a charge-carrier drift in the field that the potential difference of doped films creates across the undoped absorber region.[1] Accordingly, light trapping by means of light-scattering interface textures was demonstrated as early as 1983 by Deckman *et al.*,[5] and light management became an integral part of thin film silicon devices in the decades that followed.

Following the realization of amorphous field effect transistors by Le Comber, Spear and Ghaith[6] and their subsequent use in liquid crystal displays, photovoltaics and flat panel displays drove the development of thin film silicon technology simultaneously; the excellent in-door performance of amorphous silicon solar cells made them a suitable choice for powering pocket calculators that some of us remember from the 80s. Manufacturing on increasingly large areas enabled an economy of scale that made flat panel displays become a commodity throughout the 90s. In the 2000s, several suppliers of the display industry adapted their large area tools for solar modules, inspiring at the same time new developments in research, such as technologies for faster deposition of microcrystalline silicon or the use of doped SiO_x films for reduced parasitic absorption.[7] A snapshot of the state-of-the-art is given in Table 1.

In this contribution, we review the key elements that constitute thin film silicon solar cells and modules, and discuss some of the essential properties of the material, ensuing design rules for cell fabrication, light management, and issues of upscaling.

Ecole Polytechnique Fédérale de Lausanne (EPFL), Photovoltaic and Thin Film Electronics Laboratory (PV-Lab), Maladière 71b, CH-2000 Neuchâtel, Switzerland. E-mail: franz-josef.haug@epfl.ch

Table 1 Highest certified efficiencies of thin film silicon cells (stabilized, area ≥ 1 cm^2)

	V_{oc} (mV)	J_{sc} (mA cm^{-2})	FF	η
a-Si on transparent SnO_2 : F with texture (AIST)[8]	896	16.36	69.8	10.22
μc-Si on an Ag reflector with a hexagonal pattern (AIST)[9]	535	29.07	73.1	11.37
Tandem on transparent ZnO : B with texture (EPFL)[10]	1382	12.82	71.3	12.63
Triple junction on texture etched ZnO : Al (LG Electronics)[11]	1963	9.52	71.9	13.44

From research to manufacturing

The development of thin film silicon reflects the importance of scalable technologies. Table 1 shows that most research is carried out with devices on areas around 1 cm^2 whereas manufacturing tools in photovoltaics handle plates with sizes between 1.4 and 5.2 m^2 and further scaling to 9 m^2 has been demonstrated for display applications.[12] The underlying plasma processes are rather unique in their capability of applying equally well to small and large areas. In order to demonstrate the maturity and the level of reliability of thin film silicon, we plot in Fig. 1 the highest certified efficiencies of cells and modules with respect to the reported size of the device.[13]

In addition to the data collected in the Solar Cell Efficiency Tables,[14] we added two recently certified results that will be included in the next version, *i.e.* the a-Si/μc-Si tandem cell with efficiency of 12.6% (ref. 10) from Table 1 and a certified efficiency of 12.2% on a 1.4 m^2 module from the R&D facility of TEL Solar.[15]

Except for thin film silicon, the module results of all technologies shown in Fig. 1 are significantly lower than the respective cell results. This is particularly surprising for the crystalline technologies where the possibility to sort on the wafer level should guarantee uniform performance of all wafers that go into a module. However, there are necessarily area losses between the wafers to accommodate for series connection and thermal expansion of the ribbons upon integration into modules. We indicate these losses by dashed lines.

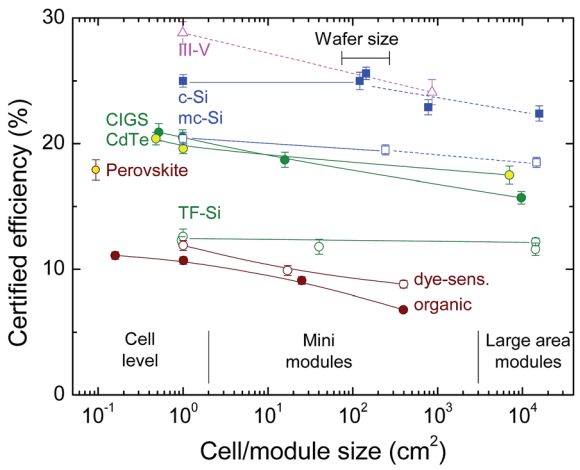

Fig. 1 Independently certified efficiencies of different photovoltaic technologies, plotted with respect to the cell or module size.[14]

For the thin film technologies, the difference between cells and mini-modules is ideally limited to the lost area of the series connection, but it can also be due to the incompatibility of process steps with large area fabrication, for example spin coating or lithography. The difference between mini-modules and production-modules generally illustrates the effect of spatial inhomogeneities of the manufacturing processes on large area. Fig. 1 illustrates that thin film silicon fares particularly well in both respects; advanced interconnection of cells by laser scribing minimizes the area losses, and the scalability of plasma reactors and deposition regimes results in very small differences between cell and module results. On the module level the efficiency-gap to the crystalline technologies, and certainly to the other established thin film technologies, is thus much less pronounced than on the cell level.

Thin film silicon

The term "thin film silicon" refers to a broad class of materials and alloys whose defining element is not so much the actual nature of silicon in the form of a thin film, but their growth procedure. Virtually all types of electronically active silicon films are grown by plasma-enhanced chemical vapour deposition (PE-CVD) from Si- and H-containing precursor gases by means of a capacitively coupled plasma within the enclosure of parallel-plate reactors. Plasma excitation usually occurs at the standard frequency of 13.56 MHz, but higher frequencies are in use because of higher deposition rates or modified dissociation chemistry of the precursor gases.[16] Films are usually grown at pressures between 0.3 and 20 mbar from silane (SiH_4) or silane/hydrogen mixtures;[17] addition of methane (CH_4) and germane (GeH_4) is used for films with higher and lower bandgaps, respectively. Doping was demonstrated for both, a-Si : H and μc-Si : H, by adding phosphine (PH_3) or di-borane (B_2H_6) to the precursor gas mix.[1,18,19] Because of issues with shelf-life, di-borane is increasingly replaced by BF_3 or tri-methyl-boron (TMB).[20,21] Generally, a-Si : H shows only moderate doping efficiency because the doping process, more precisely the accompanying shift of the Fermi-level, results in the creation of additional defects and makes the doping-process self-limiting.[22,23] Microcrystalline silicon can be doped more efficiently[19] and is therefore used for internal junctions and contacts to external circuitry, adding the benefit of its higher transparency.

Compared to crystalline silicon with its well-ordered fcc structure, thin film silicon is either amorphous (a-Si : H) or microcrystalline (μc-Si : H), and it contains a substantial

amount of hydrogen that is incorporated during the deposition. Usually "thin film silicon" extends also to alloys with germanium or carbon as well as compounds with oxygen and nitrogen of varying stoichiometries.

Thin film silicon covers bandgaps of 1.1 eV (microcrystalline Si) and 1.7 eV (amorphous Si) and is thus ideally suited for integration into tandem solar cells.[24] Likewise, alloying of amorphous Si with 30% Ge allows lowering the bandgap to *ca.* 1.5 eV; higher Ge-contents are not recommended because they reduce the electronic quality. Since materials with different bangaps can be fabricated in the same reactors and from similar precursor gases, single-junction cells with a low gap are not directly upscaled into modules, but they are usually integrated into tandem or triple-junction devices because these are more advantageous in terms of higher cell potential and lower cell current. Only these multi-junction cells are subsequently processed into modules on a large area as shown in Fig. 1.

Amorphous silicon

Amorphous silicon maintains a tetrahedral bonding environment on a range of three to five next-neighbours[25] which makes its absorption resemble the indirect characteristic of crystalline silicon rather than the one of direct semiconductors. However, the disorder on medium- and long-range suppresses the formation of sharp band edges; instead there is a so-called mobility gap of *ca.* 1.7 eV between the extended states of the valence- and the conduction-band, accompanied by tails of localized states that do not contribute to charge transport but act as shallow trap-states. In hydrogen-free materials, there are *ca.* 10^{20} cm^{-3} unpaired dangling bonds that translate into deep defect states close to the middle of the gap, thus acting as recombination centres.[26] If the films are grown from silane by PE-CVD, the majority of the defects are passivated with hydrogen, resulting in defect densities between 10^{15} and 10^{16} cm^{-3} in state-of-the-art materials.[27] The necessity to hydrogenate the material defines thus an optimum range of deposition-temperatures between 180 and 270 °C. Lower temperatures cannot provide enough thermal energy for surface diffusion of the arriving radicals and thus impede the formation of tetrahedral bonding; higher temperatures facilitate hydrogen desorption which ultimately deteriorates the passivation of dangling bonds with hydrogen.[28,29]

A particular property of amorphous silicon is light induced degradation (LID) first reported by Staebler and Wronski;[30] they found that the photoconductivity decreases upon continuous illumination, and observed a complete recovery of the initial state by annealing. A variety of further experiments suggested that the photoconductivity is reduced by additional dangling-bond defects which are not created by the illumination itself, but by the recombination of charge carriers, regardless of whether they are photo-generated or otherwise injected.[31,32] The underlying mechanisms were topic of lengthy debates throughout the 80s[33–37] and a renewed interest in the 2000s[38–43] which made it more and more clear that defect creation is related to bonds at internal surfaces of nano-sized voids or multi-vacancies.[44–46] Whereas an ultimate understanding is still elusive, it is nevertheless established that the effect saturates for practical time-scales at *ca.* 10^{17} cm^{-3} in state-of-the-art materials,[33,47] and that it is reversible over hundreds of illumination–annealing cycles. In solar cells, the impact of LID is less pronounced in thinner devices;[48,49] state-of-the-art devices with absorber layer thickness between 200 and 220 nm stabilize thus at typically 85–90% of the initial efficiency.[50,51] In order to avoid confusion, the independently certified efficiencies of thin film silicon solar cells are always measured in the stabilized state. As a matter of fact, ref. 14 mentions that stability has not been explicitly investigated for the other thin film devices shown in Fig. 1.

Microcrystalline silicon

Microcrystalline silicon is a mixed-phase material that consists of small crystallites which are embedded into a matrix of amorphous silicon. The high density of surface states is effectively passivated by the matrix material. Owing to the size of the crystallites, it should be more appropriately called nanocrystalline silicon (nc-Si : H); however, its size variation between 3 and 10 nm is generally too large to yield noticeable effects of quantum confinement. The bandgap is thus similar to crystalline silicon and the material exhibits no noticeable LID effect.[52]

Microcrystalline materials can be grown from the same gases as amorphous silicon, *i.e.* silane and hydrogen, but generally higher power density[19] or a high content of hydrogen beyond 80 or 90% is needed.[53] Alternatively, the equilibrium between gas supply and pumping speed can be tuned towards depleted high-pressure regimes where microcrystalline silicon can be deposited even from pure silane.[54,55] Recently, microcrystalline films deposited from SiF_4 attracted attention because the content of the amorphous matrix can be significantly reduced with respect to materials grown from silane.[56]

Device design

The particular electronic properties of thin film silicon necessitate attention during device design:

- Since doping also creates defects, device designs on the basis of p–n junctions cannot be applied. Instead, p–i–n junctions are used where doped layers create a drift-field across the undoped absorber layer. With a potential difference between the doped layers of *ca.* 1 eV, the amorphous absorber layer should be kept in the range of *ca.* 200 nm in order to create a strong drift-field for carrier extraction. For μc-Si : H, thicknesses of *ca.* 3 to 4 μm are tolerable,[57,58] but not desired in terms of production throughput.
- Holes have lower charge carrier mobility than electrons. Combined with the fact that typical illumination conditions yield a high density of photo-generated carriers at the front interface, illumination should occur through the p-layer. Holes created close to the p–i interface are thus majority carriers and they need to drift only a short distance; electrons with their higher mobility can drift over a larger distance to the opposing electrode. For μc-Si : H, also this constraint is relaxed and cells with good collection upon n-side illumination have been presented.[59]

• The high defect density within the doped layers leads to a fast recombination of minority-carriers. Photo-generation in these layers should be avoided by increasing their bandgap[60] and by reducing their thicknesses to the minimum that is required for the drift field.

• The existence of tail states leads to increased recombination when the quasi Fermi-levels are split under forward bias. This limits the attainable open circuit voltage and the fill factor below the theoretical limits of p–i–n junctions.[2,61]

In the context of manufacturing, the name p–i–n not only refers to the type of junction, but also to a deposition sequence where the p-layer is deposited first. This is opposed to the n–i–p structure where the n-layer is grown at the beginning of the deposition process.

Light management

Charge carrier transport puts an upper bound to the feasible absorber layer thicknesses for cells based on a-Si : H and μc-Si : H. However, these thicknesses are too small for efficient absorption of light with energy close to the bandgap.

This appears to result in a fundamental incompatibility between optics and electronics of the solar cell; the light path should be as long as possible for full absorption whereas the distance between the electrodes should be as short as possible for an efficient collection of charge carriers. In essence, light should do a sharp turn from its incident angle into the plane of the absorber.

Incidentally, the same issue applies to crystalline silicon where wafer thicknesses of 300 μm are still insufficient for full absorption. It is thus also c-Si technology where the issue was first addressed.

Light path enhancement – inspiration from c-Si technology

In c-Si wafers, prolonging of the light path is achieved by facets on the surface that refract incident light into oblique angles[65] as illustrated in Fig. 2. For regular arrays of facets, Campbell and Green applied ray-tracing and found path-enhancement up to 70-fold for their optimized pattern; however, this value is only obtained for a small range of incident angles.[66] For random surface facets, Yablonovitch and Cody proposed a statistic treatment analogous to the equi-partition theorem, arguing that the intensity of weakly absorbed light becomes uniformly distributed between all available modes inside and outside the absorber.[67] Using the mode-density of black-body radiation, they derived an upper limit of the path enhancement equal to $4n^2$, n being the refractive index of the absorber layer.[68] In case of c-Si this evaluates to just above 50 in the weakly absorbing region, and it applies to all angles of incidence.

As a word of caution it should be mentioned that the theoretical limits are usually determined on the basis of idealized structures, by assuming loss-free supporting layers, if any, perfect anti-reflection condition on the front and perfect reflectors at the back, *etc.* Fig. 3 shows that even for fairly ideal structures like the PERL-[62] and HIT-cells,[63] the enhancement in the very weakly absorbing region is around 25 to 30 instead of 50.

Light path enhancement in thin film cells

When light scattering textures are applied in thin film solar cells, the size of the textures must be reduced along with the absorber thickness. This leads to two important differences in the theoretical description; firstly, it is no longer adequate to describe the absorbing film with the continuous density of the black body; instead, the formation of discrete waveguide modes and their confinement to the guiding medium have to be taken into account.[69,70] Secondly, refraction at ever smaller facets is eventually replaced by scattering effects.[5] Likewise, making regular arrays ever smaller will produce diffraction effects as soon as the period becomes comparable with the wavelength.[71] Gratings can be engineered to compress the mode-density for certain spectral regions, pushing the theoretical path length enhancements up to $4\pi n^2$ and $8\pi n^2/\sqrt{3}$ for dielectric configurations of square and hexagonal geometry, respectively.[72] Similar to the case of regular arrays treated with geometric optics, these limits apply only for a narrow range of angles close to perpendicular incidence and are hence of limited use in static outdoor application.

A different strategy to densify the modal distribution uses surface plasmon polaritons (SPPs) which are formed at the interface between dielectrics (*i.e.* the absorber) and metals (*i.e.* the reflecting back electrode). The SPP of the silicon/silver interface has attracted particular attention, not only because silver is an excellent reflector, but also because the energy of the resonance coincides exactly with the weakly absorbing region of silicon.[73,74] However, interfaces between metals and

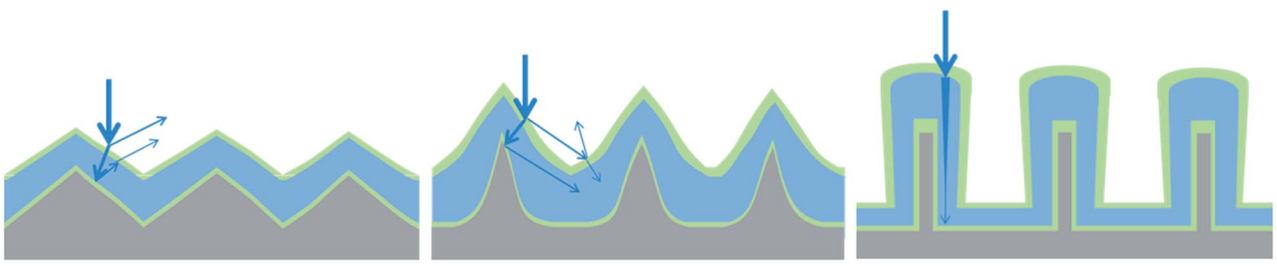

Fig. 2 Illustration of light scattering textures in solar cells. Shallow structures (left) are prone to reflection losses whereas textures with higher aspect ratios permit forward scattering with second incidence on the cell (middle). Nano-wire designs have the potential for axial absorption paths much longer than the radial film thickness (right).

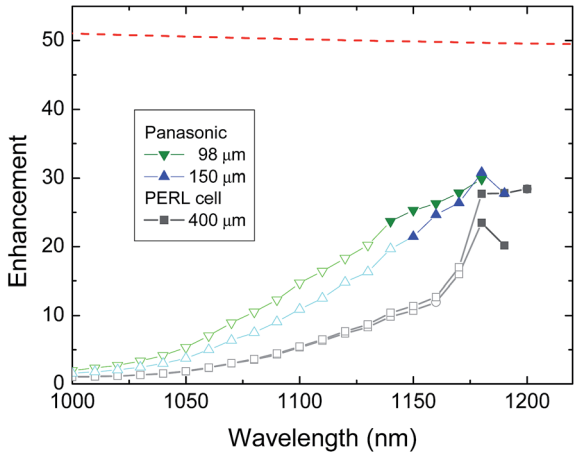

Fig. 3 Light path enhancement F of different crystalline silicon solar cells,[62,63] estimated as the ratio between the EQE and αd, the absorption of a single light pass. This estimate holds only in the very weakly absorbing region as illustrated by the full symbols. The dashed line illustrates that the $4n^2$ limit of c-Si is close to 50.[64]

semiconductors are notoriously defective,[75,76] and amorphous silicon is no exception in this regard.[77] Therefore, virtually all solar cell designs with metallic back reflectors integrate a thin buffer layer at the interface,[78,79] and reflectors with much reduced loss on the basis of fully dielectric Bragg reflectors have been suggested.[80,81]

A simple yet powerful model for assessing the light path enhancement was proposed by Deckman *et al.*;[5,82] assuming full randomization and a simple ray-tracing approach; they describe the path enhancement upon each passage through the film by an infinite sum that converges to a simple analytic formula. The approach includes parasitic absorption in supporting layers and applies not only to weak, but also to strong absorption. Moreover, it can be generalized for different degrees of randomization during the first scattering event which is the most important one.[57] The intuitive power of the ray-tracing approach inspired the development of more detailed models that treat coherent and incoherent propagation of light and take into account the scattering processes at each individual interface.[83–85] Among the most important results that can be drawn from these detailed models is the insight that the optical system with random interface scattering is already very advanced and that absorption in the doped layers and in the electric contacts represents a dominant parasitic loss whose reduction calls for continued research efforts.[57,86–88]

Light scattering surface textures

Deckman *et al.* did not only present a powerful theoretical treatment for absorption enhancement in thin film solar cells,[5] they also presented several pioneering experimental results:

• They manufactured textured interfaces by spin-coating monolayers of self-organized spheres consisting of materials such as alumina or polystyrene and sizes between 300 and 800 nm; subsequently, they either deposited through the openings between the spheres, or applied reactive ion etching.[89] In today's parlance the process is called nano-sphere lithography and it developed into a very versatile procedure of micro- and nanofabrication.[90–92]

• They found an optimum period for amorphous solar cells in the range from 400 to 600 nm.[93] Modelling work of amorphous solar cells with 2D periodicity confirmed this range of periods.[80,94,95]

• They reported on the beneficial effect of either inserting a buffer layer between silicon and the metal, or even detaching the reflector from the solar cell altogether.[82] All modern cell designs with metallic back reflectors use a buffer layer, typically made from ZnO.[58,96,97] The presence of a buffer layer with a low refractive index was found to suppress the excitation of the SPP resonance at the interface between silicon and silver.[98] Whereas suggested to be beneficial for absorption enhancement in terms of their modal density,[73,99] the electromagnetic field of SPP resonances peaks at the interface. In conventional cell designs, the resulting absorption enhancement extends thus over one of the doped layers which do not contribute to the photo-current (Fig. 2).

• Even though they used an n-illuminated structure, they were able to note the importance of a good back reflector like silver and the advantage of keeping the silver layer flat.[5] Since silver is one of the best reflector materials, it is desirable to reduce parasitic absorption of its SPP resonance by using either flat interfaces where their excitation is prevented by simultaneous conservation of energy and momentum, or by using buffer layers of adequate thickness.[96,100]

• Finally, they also noted that the natural texture of transparent conducting oxide (TCO) surfaces like F-doped SnO_2 can already provide a certain degree of enhancement.[5]

Textured front TCOs for superstrate cells

For large area manufacturing, the latter aspect, *i.e.* formation of natural textures, developed into the most successful and most widely used mechanism for absorption enhancement. Typically, texture is introduced into the contact layer that precedes the growth of the absorber. In the p–i–n configuration, often called the superstrate-configuration, because illumination occurs through the glass which is thus "above" the active layers, the surface of the TCO is textured. The development of a pyramid-shaped surface texture is well documented for SnO_2 deposited by the CVD method (AP-CVD) from precursors of $SnCl_4$ and H_2O.[101,102] Fig. 4 shows the texture of "Asahi-U", the type of

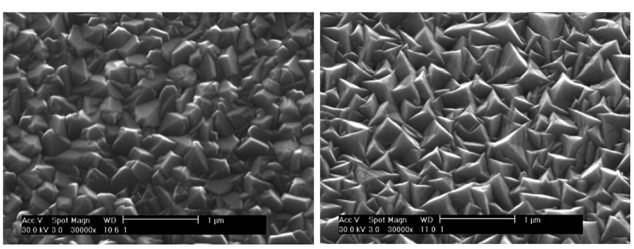

Fig. 4 Surface morphologies of Asahi-U SnO_2 : F (left) and 2 μm thick ZnO : B (right). Scale bar: 1 μm.

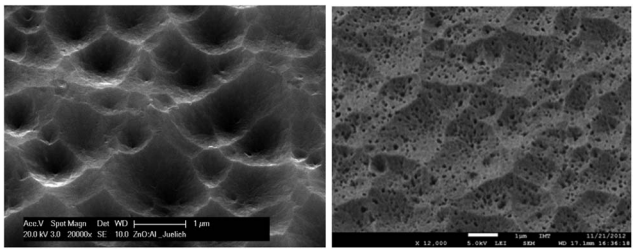

Fig. 5 Surface morphologies of ZnO : Al etched in HCl (left) and doubly etched in HCl and subsequently in HF.[115,116]

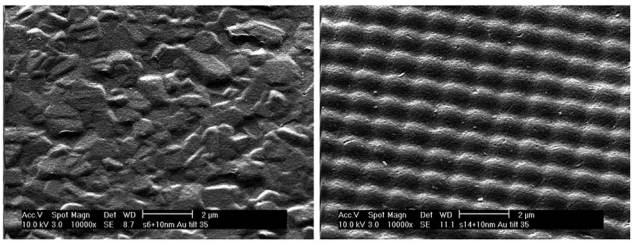

Fig. 6 Surface textures obtained by imprinting into a UV-curable resin. The left panel is a copy of the random surface facets of silver deposited at an elevated temperature; the right panel shows a 2D-sinusoidal grating with a period of 1200 nm. Scale bar: 2 μm.

fluorine doped SnO_2 : F that is most widely used in research and development.[103,104]

A similar surface texture is obtained on ZnO : B grown by low pressure CVD (LP-CVD) from precursors of diethyl-zinc and H_2O; the conductivity is easily controlled by using di-borane as the dopant source.[105,106] ZnO is particularly attractive for thin film silicon because it is stable in hydrogen-rich plasma whereas the reduction of SnO_2 or In_2O_3 yields a metallic layer at the interface which results in parasitic absorption.[107–109]

An AFM analysis of the films shown in Fig. 4 reveals that the mean tilt angles with respect to the surface normal are *ca.* 30° and 45° on the textures of Asahi-U and LP-CVD ZnO, respectively. Since steeper facets scatter light more efficiently,[110,111] the Asahi glass company introduced in 2009 the VU-type that features steeper facets and lower doping; they also provide the W-type which consists of a double texture.[112,113] However, strong roughness can also create issues for cell processing; assuming that arriving radicals undergo surface diffusion before they build up the film, valleys are likely to accumulate materials with inferior quality because surface diffusion is impeded by the geometry.[114]

Alternatively, a light scattering texture can also be obtained after deposition. For example, sputter-deposited ZnO can be etched easily in diluted HCl. Depending on the deposition conditions, etch pits with a wide variety of sizes and opening angles can be obtained.[117,118] The different types of craters that are etched by HF[115,116] can then be used to create modulated double-structures as shown in Fig. 5.

Textured back contacts for substrate solar cells

The development of light scattering textures is different for the n–i–p configuration, also called the substrate-configuration. Since the substrate is at the back of the device, it does not need to be transparent. Instead, it can be coated with highly reflecting metals like silver or aluminium. If the coating is carried out at high temperatures between 300 and 400 °C, these metals develop natural surface textures that are well adapted to light scattering.[119–121] The n–i–p configuration is thus normally applied to flexible solar cells on steel foils (the approach used by UniSolar and Xunlight) or polyimides (Fuji) because these materials resist the deposition temperatures of the back reflector. Also here, the development proceeded largely by empiric developments because the shape of the initial texture becomes modified during the growth of the absorber film.

An alternative to costly high-temperature substrates came with the development of holographic imprinting on a large scale during the mid-2000s. Since the desired textures can be imprinted, it is no longer needed to deposit the back reflector at high temperature for texturing. Instead, low-cost substrates like polyethylene-terephthalate (PET) and -naphthalate (PEN) can be used because they tolerate temperatures up to 150 and 180 °C, respectively, making them compatible with PECVD processing of thin film silicon.[122,123] For example, the two textures in Fig. 6 were imprinted into a UV-curable resin on top of a flexible PEN substrate, illustrating that imprinting offers also the additional freedom of choosing any arbitrary texture, not only natural ones.[124]

Light scattering by metallic nano-particles

Metallic nano-particles have attracted much interest because they can sustain highly localized oscillations of the free carrier plasma which coined the term "plasmonics".[125] Their radiation pattern closely resembles those of idealized dipoles[126] and they yield extraordinary enhancement of the electromagnetic field in the vicinity of their surfaces.[127] Application in solar cells dates back to Stuart and Hall who designed a pioneering experiment[128] and also gave an enlightening interpretation;[129] they used a crystalline silicon-on-insulator (SOI) structure consisting of a 160 nm thick silicon absorber that is separated by a 190 nm thick SiO_2 layer from the underlying silicon wafer. After diffusing a laterally collecting junction into the silicon film, they evaporated thin films (10 to 12 nm) of Cu, Ag, and Au on top of a 30 nm thick spacer layer of LiF. Nano-particles were formed from these metal films by coalescence in a subsequent annealing step.

The results in Fig. 7 show that this configuration resulted in 3-, 5-, and 12-fold enhancement of the collected photocurrent for Ag-, Au-, and Cu-particles, respectively. Variation of the size showed enhancement up to 18 for Ag-particles, *i.e.* about 40% of the $4n^2$ limit.[130]

Regardless of the type of metal or the particle size, their experiment showed the strongest enhancement always in the range between 700 and 900 nm, accompanied by weaker signatures at wavelengths of 525 and 600 nm. Below these wavelengths, the "enhancement" is less than unity, *i.e.* absorption losses of the nano-particles are dominant. In a separate experiment they found that their Ag-, Au-, and Cu-

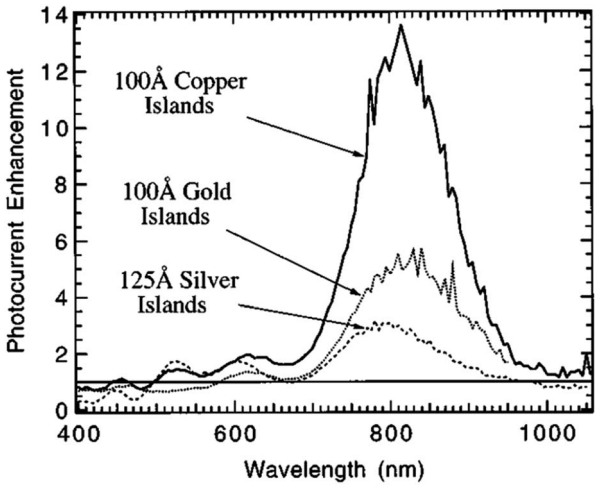

Fig. 7 Measured photocurrent enhancement due to the presence of metallic nano-particles (from ref. 128).

particles resonate at very different wavelengths of *ca.* 400, 550, and 700 nm, respectively, suggesting that there is little correlation between the wavelengths at which absorption is enhanced and those at which the particles resonate. This surprising observation is explained by the underlying coupling process. Regarding the particles as a coupled array of dipole antennas which is driven by the external field, the particles will exchange energy *via* the underlying film. In their experiment, this occurs at 750 nm because the film supports the TE1 waveguide-mode at this wavelength.[129] The enhanced photocurrent is therefore a mere side-effect of the transport of exchange-energy through this mode. Unfortunately, the authors do not analyse the photocurrent enhancement with respect to the total absorption of their system because Cu should be the lossiest of the three studied metals.

We next turn to the extent of enhancement which is related to the resonance frequency of the particles as well as to the number of particles that are coupled. Fig. 7 shows that Cu-particles yield the strongest response at 750 nm and at 600 nm because their resonance is nearest to these wavelengths. The other metals couple more efficiently to waveguide-modes at shorter wavelengths which are closer to their own resonances. From Fig. 7 it becomes clear that the second effect, the number of interacting particles, is the dominant influence; looking again at the two waveguide modes at 600 and 750 nm excited by Cu-particles, the latter is much stronger even though the broad resonance of Cu-particles at 700 nm should cover both. Stuart and Hall relate this observation to the number of particles that a given mode can couple *via* its attenuation length.[129]

This interpretation is corroborated by Pillai *et al.*[131] for a thicker film that supports more waveguide-modes. Nevertheless, the spectral variation of absorption enhancement is similar, *i.e.* below unity at short wavelengths and peaking at *ca.* 15 to 18 in the weakly attenuated region. Individual modes are no longer resolved in case of bulk-samples, but it can be shown that a dipole located at the interface between two media will radiate preferentially into the medium with a higher refractive index; in case of silicon this asymmetry can amount to almost 98%.[132]

For a given metal, larger particles resonate at longer wavelengths,[130,131] not so much because of retardation effects but more likely because of their increasingly irregular shape.[127,130,133] In all cases, the size should not exceed the incident wavelength, otherwise weaker quadrupole oscillations will be excited.[130] Another way to tune the resonance frequency is *via* the dielectric environment, for example by using spacer layers of a higher refractive index such as Si_3N_4 or TiO_2.[134]

We note that quoting values of an enhancement in a small spectral region can be misleading if they are not referenced to the integrated absorption in the film. For a thin silicon-film of 160 nm without anti-reflection coating like the one underlying Fig. 7, the absorption below 500 nm averages at *ca.* 30%, but it is only 0.5% at 800 nm. Multiplied with respective enhancement factors of 0.8 and 12, we end up with 24% at short wavelengths and 6% at long wavelengths, *i.e.* in terms of absorption there is little or no gain in the integrated absorption. In complete devices, the loss of photocurrent for visible wavelengths can be much larger than the gain in the weakly absorbing region.[134]

Compared to wafer-based technology where particles have been tested mostly at the front, thin film silicon offers more freedom. Parasitic absorption of visible light can be avoided by incorporating the particles closer to the back reflector. Various positions have been tested, either within the absorber layer,[135] between the component cells of a tandem configuration,[136] at the interface between the n-layer and the dielectric buffer layer of the back electrode,[137] or within the buffer layer[138] which is a benign position that avoids the defective metal/semiconductor interface. Nevertheless, the particles should be as close as possible to the absorber,[139] confirming that near-field effects are responsible for the enhancement.

An additional difficulty in identifying the advantage of plasmonic particles is the fact that their incorporation also introduces a texture. The results cited so far put the absorption enhancement for textures as well as the one of plasmonic scatterers at about half of the $4n^2$ limit. A direct comparison of a nano-particle based reflector with an Ag-coated Asahi-U texture found a slight improvement with the plasmonic approach,[140] but the different shapes of the light scattering textures prevent a conclusive comparison. A dedicated experiment where silver particles and a textured silver reflector were defined by lithography with equal particle-size and -shape found the conventional design with a textured Ag reflector more advantageous.[141,142] Noticeably though, none of the structures using plasmonic effects could reach state of the art light trapping as obtained with a rough front TCO and a TCO/metal or TCO/dielectric rear reflector. It appears that, in the end, parasitic losses induced by the metal prevail over the potential gains.

3D designs for solar cells

The whole dilemma of combining a long light-path and a short collection length could be elegantly resolved by 3D designs. Using radial junction geometries such as nano-wires oriented parallel to the incident light, Fig. 2 illustrates that absorption

can take place along the full length of the wire whereas charge carrier collection can proceed along a relatively short path along the radial direction. Consequently, the design of nano-wire solar cells received much attention from theoretical and experimental sides. As in the previous sections, we would like to emphasise the development of devices based on thin film silicon in this section.

Nano-wire solar cells based on amorphous silicon also use p–i–n or n–i–p junctions, but the rule of placing the p-layer at the front of the device is not as strict as in devices with interface texture. Illumination through the n-layer can be accepted since the intended side-wall thicknesses are often in the region of *ca.* 100 nm and can thus still allow an efficient hole-collection.

Arrays of opaque nano-wires for solar cells have been manufactured by reactive ion etching (RIE) of tapered pillars into a c-Si substrate,[146] or by catalytically growing multi-walled carbon nanotubes on patterns of Ni-islands.[90,150] Usually, such pillars are covered with a metal-layer for better conductivity and reflectance, followed by the deposition of n–i–p[146] or p–i–n[151] structures and a front electrode. Alternatively, nano-wires with cores made from silicon were proposed because they are fully compatible with the steps of solar cell manufacturing and offer thus a simple and lean processing sequence.[147] In this case, nano-wires are grown by a vapour–liquid–solid (VLS) process on nucleation templates made by coalescence from a thin evaporated film of tin. Even this step can be simplified by starting from a thin ITO film that is reduced in H_2 plasma and subsequently annealed to form the nucleation template by coalescence. Then, a radial junction can be deposited on such nano-wires by simply switching the growth mode to the conditions of amorphous silicon.[147]

If illumination should occur through the supporting superstrate, the nano-wires must be made of a transparent conducting material. Experimental demonstrations used ZnO and e-beam lithography, either to define a hexagonal pattern of cylindrical holes in a photoresist for subsequent filling with ZnO by atomic layer deposition (ALD),[152] or to etch arrays of pillars or holes into a thick ZnO starting layer.[153]

In all approaches with tall nano-wires, uniform side-wall coverage is an issue,[91] especially if small distances between the nano-wires impede the arrival of radicals from the plasma. This is either taken care of by tapering the wires,[146] or by filling in the volume between the wires altogether.[152] However, the latter approach misses out on a substantial advantage of the nano-wire design for amorphous silicon absorbers because thin absorber layers not only collect charges more efficiently, but also suffer less from LID, typically only 6–8%.[146,147,151]

Overall, manufacturing of nano-wires with very high aspect ratios often involves one or more additional processing steps, and fabrication of solar cells on these structures remains challenging. In the meantime, pillar- and cone-structures with the aspect ratio around one have already demonstrated great potential for absorption enhancement. Table 2 shows that their better compatibility with processing of thin film silicon resulted in devices that compete closely with the highest state-of-the-art efficiencies. Among these, cone-like structures were found particularly useful to direct light from perpendicular incidence into the substrate plain. Efficient cells of p–i–n type were thus

Table 2 Parameters of amorphous silicon solar cells, selected to represent the means of absorption enhancement discussed in the text. Except for the independently certified results of the first two entries (denoted in bold), all values are cited as given by the authors

Cell type	V_{oc} (mV)	J_{sc} (mA cm^{-2})	FF	η	Thickness (nm)	Comment/Ref.
Best reported devices, all on natural textures						
p–i–n on LP-CVD ZnO	885	17.94	71.92	11.4 ini	250	Sample #3497 (ref. 14 and 143)
	877	**17.28**	**66.6**	**10.1 st**		
p–i–n on Asahi-VU	901	16.55	75.7	11.3 ini	*ca.* 210	Deposited in a triode reactor,[144] similar to
	906	**16.05**	**69.5**	**10.1 st**		the cell of Table 1
n–i–p on hot Ag	992	14.65	73.0	10.6 ini	n.a.	On a flexible substrate with textured Ag film[145]
	965	14.36	67.2	9.3 st		
Cell designs with plasmonic nano-particles						
n–i–p on a textured reflector	810	15.1	64.5	9.4 ini	300	Comparison of Ag/Asahi-VU texture
n–i–p on a plasmonic reflector	810	14.8	65.2	9.3 ini		and Ag nano-particles[140]
n–i–p on a textured reflector	927	14.0	67.3	8.7 ini	200	Comparison of nano-texture and nano-particles,
n–i–p on a plasmonic reflector	936	13.5	70.9	8.9 ini		identical in size and shape[141]
Cell designs on nano-wires with a high aspect-ratio						
n–i–p on Ag-coated nano-wires	893	13.9	65.9	8.2 ini	90	Coaxial design on Ag coated Si nano-wires, 8% LID[146]
i–n on p^+ nano-wires	796	15.4	62.9	7.7 ini	100	Cell on Si p^+-core, no metallization, 6% LID[147]
	782	14.9	62.2	7.2 st		
Cell designs on textures with a moderate aspect-ratio						
n–i–p on nano-domes	955	14.9	68.1	9.7 ini	200	Hexagonal array with an optimum
						period of 350 nm (ref. 91)
p–i–n on nano-cavities	915	17.1	69.6	10.9 ini	200	Comparison of random and periodic
p–i–n on random pyramids	913	17.1	69.7	10.9 ini		textures in co-deposition[148]
p–i–n on flat ref	914	12.0	72.4	7.9 ini		
n–i–p on nano-spikes	866	14.7	65.9	8.4 ini	140	Anodically etched Al substrate[149]

demonstrated on transparent templates by direct etching with a defined uner-cut into the glass substrate,[91,154] by nano-imprinting of adequate morphologies into a UV-curable transparent resin,[148] or by hydrothermal growth of ZnO which can be tuned to yield pillar- or cone-shapes.[155] Likewise, n–i–p devices were demonstrated on etched quartz substrates[91] and anodically etched arrays of Al-spikes.[149]

Textures for microcrystalline silicon and tandem solar cells

The measures for absorption enhancement in microcrystalline solar cells follow largely the same principles as those for amorphous absorbers except that the smaller bandgap of microcrystalline silicon necessitates scattering of longer wavelengths and thus larger feature size.[58,160–163]

The design of textures for microcrystalline cells must take into account that the material is more vulnerable to rough substrates than amorphous silicon.[164–166] The V-shaped valleys visible between the pyramids in Fig. 4 were identified to nucleate material of inferior quality which results in local "shunt" paths. Microcrystalline absorbers are therefore rarely applied on extreme structures like nano-wires. Since a minimum level of substrate texture is nevertheless mandatory for absorption enhancement, there are two major directions of development. The textures are adapted to avoid the sharp features,[58,117,160] compensating thus a lower level of absorption by better electrical performance. Alternatively, the PECVD can be adapted in order to grow denser material that is less sensitive to the substrate roughness.[167] Finally, additional functional layers can be built into the cell to mitigate the shunting problem.[168,169]

In tandem cells, light scattering should be tailored to the different wavelength ranges of the component cells. This inspired the fabrication of multi-scale textures, for example by etching a large texture into the glass substrate and to add the natural texture of the front electrode.[170] Instead of etching, an appropriate texture with large features can also be imprinted into a UV-curable resin applied to the glass substrate.[171] Alternatively, the double structure in Fig. 5 has been obtained by combining the different shapes of craters that HCl and HF etch into sputtered ZnO.[172] Likewise, the large features of thick LP-CVD ZnO films can be combined with smaller features of an additional, thinner film if local epitaxy is broken by the insertion of a thin SiO_x layer (Fig. 8).[173,174]

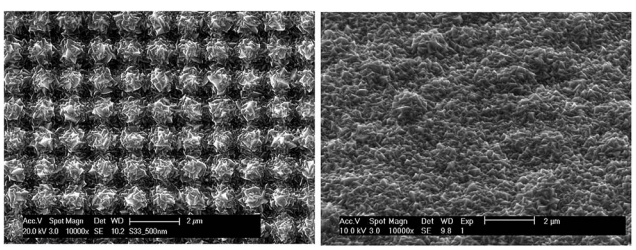

Fig. 8 Fine grained textures of ZnO grown by LP-CVD, grown on a texture obtained by imprinting in a UV-curable resin (left)[171] or on ZnO with large texture after breaking local epitaxy (right).[173]

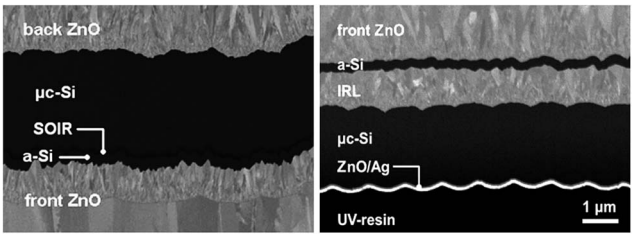

Fig. 9 SEM cross-sections of tandem cells. The left panel shows a p–i–n tandem cell on a doubly textured ZnO front electrode with a silicon oxide intermediate reflector (SOIR, illumination from the bottom).[174] The right panel shows an n–i–p tandem cell on a periodic back reflector with textured ZnO as the intermediate reflector layer (IRL, illumination from the top).[177]

An altogether different approach incorporates the texturing schemes at different stages of the tandem process. Since the amorphous top cell tolerates a higher roughness than the microcrystalline bottom cell, a smoothening interlayer can be inserted between the component cells.[175,176] For n–i–p tandem cells, this concept has to be applied in the opposite sense since the bottom cell is deposited first. Fig. 9 shows that starting from a moderate texture with a large scale, an interlayer of textured ZnO can be used to develop a natural texture on a smaller scale that is appropriate for the top cell.[177,178]

Triple junctions and beyond

The concept of tandem junctions is readily generalized to three or more junctions. Thin film silicon is a versatile material whose integration into multiple junctions poses few restrictions from the process side. Indeed, the first quadruple and quintuple cells on the basis of amorphous silicon have been demonstrated as early as 1979 in order to produce higher output-voltage than single junction cells.[179]

More recent efforts towards triple (and very lately also towards quadruple cells) were carried out with the objective to find ideal distributions of the photocurrent among the junctions. Starting from current densities around 30 to 32 mA cm^{-2} that can realistically be drawn with a microcrystalline absorber layer of acceptable thickness (*c.f.* Table 3), an equal distribution in a tandem cell would necessitate an amorphous sub-cell with 15 to 16 mA cm^{-2}. Table 2 suggests that amorphous cells can achieve this value easily, but it should be noted that these cells use a back reflector. In a tandem cell, only one scattering event at the front can be exploited, light that arrives at the back of the top cell gets transmitted into the bottom cell and is eventually absorbed there. Consequently, top cell currents are limited to *ca.* 10 to 11 mA cm^{-2}. The issue has been resolved by the introduction of the intermediate reflector layer (IRL) that yields a partial reflection of light at the interface between the two sub-cells.[7,180–182]

Alternatively, 30 mA cm^{-2} can be distributed more easily between three cells of a triple junction, either true triple cells with three different band gaps,[183,184] or devices that combine an amorphous top cell with a microcrystalline tandem at the bottom.[185–187]

Table 3 Parameters of selected microcrystalline silicon solar cells. Bold entries denote independently certified results

Cell type	V_{oc} (mV)	J_{sc} (mA cm^{-2})	FF	η	Thickness (μm)	Comment/Ref.
Certified record devices						
n–i–p on a honeycomb, ZnO front	**535**	**29.07**	**73.1**	**11.4**	**n.a.**	Hexagonal texture defined by lithography[9,156]
n–i–p on a honeycomb, ITO front	**542**	**27.44**	**73.8**	**11.0**	**1.7**	
p–i–n on LP-CVD ZnO	**549**	**26.55**	**73.3**	**10.7**	**2**	ZnO subjected to Ar treatment[157]
n–i–p on a hot Ag, ITO front	**539**	**24.35**	**76.8**	**10.1**	**2**	Aperture area, including shading of grid[158]
High V_{oc} cells						
p–i–n on LP-CVD ZnO	608	19.7	77.1	9.8	0.6	High V_{oc} with amorphous n-buffer, no AR coating[157]
p–i–n on HCl-etched ZnO	585	19.8	72.4	8.4	n.a.	High V_{oc} with HW-buffer[159]

Finally, the recent experimental demonstration of quadruple junctions leaves yet more liberty with current matching,[188,189] and it provides a basis for broader spectral utilization with high-gap absorbers like amorphous SiC[190] or SiO_x[188,191] and low-gap absorbers such as microcrystalline SiGe alloys.[192,193] Modelling of such devices predicts realistic pathways for efficiencies up to 16%, and beyond that if parasitic absorption losses can be controlled better than today.[194]

Conclusions

Thin film silicon is a very mature and reliable material for photovoltaics with many years of proven outdoor performance. Because of its moderate efficiencies it lost in market share in the competitive environment of the last five years, but it still maintains its main advantages of low-cost manufacturing and aesthetically pleasing products.

Owing to the indirect nature of the band-gap, light management was a key throughout the development of thin film silicon based photovoltaics, and it reached a very mature level. Over the last decade, the major improvement in cell current and efficiency has come from the reduction of parasitic light absorption with improved TCOs and with the introduction of doped SiOx : H layers that can be made more transparent than the carbide layers used earlier.

Thin film silicon is a versatile and unobtrusive technology that has traditionally been applied very early to new concepts like flexible substrates, imprinted textures, and novel light-management schemes like nano-pillars or plasmonics. Nevertheless, random structures still provide the best current-densities and yield thus the highest device efficiencies. With regard to theoretical understanding as well as to large-area manufacturing, light management probably reached its most advanced level in this technology. Thin film silicon will thus maintain its place in the research landscape, and it will continue to contribute to the production of solar energy.

Acknowledgements

We thankfully acknowledge funding within the EU FP7 project FastTrack (no. 283501) and by the Swiss Federal Office of Energy (SI/500750-01).

References

1 W. Spear and P. Le Comber, *Philos. Mag.*, 1976, **33**, 935–949.
2 D. E. Carlson and C. R. Wronski, *Appl. Phys. Lett.*, 1976, **28**, 671–673.
3 R. C. Chittick, *J. Non-Cryst. Solids*, 1970, **3**, 255–270.
4 R. Loveland, W. Spear and A. Al-Sharbaty, *J. Non-Cryst. Solids*, 1973, **13**, 55–68.
5 H. W. Deckman, C. R. Wronski, H. Witzke and E. Yablonovitch, *Appl. Phys. Lett.*, 1983, **42**, 968–970.
6 P. Le Comber, W. Spear and A. Ghaith, *Electron. Lett.*, 1979, **15**, 179–181.
7 T. Sawada, Y. Koi, T. Sasaki, M. Yoshimi, M. Goto and K. Yamamoto, US patent, 2006/0174935, 2006.
8 T. Matsui, A. Bidiville, H. Sai, T. Suezaki, M. Matsumoto, K. Saito, I. Yoshida and M. Kondo, presented at the 6th World PVSEC, Kyoto, 2014.
9 H. Sai, T. Matsui, T. Koida, M. Kondo, S. Nakao, Y. Takeuchi, H. Katayama and I. Yoshida, presented at the 6th World PVSEC, Kyoto, 2014.
10 M. Boccard, M. Despeisse, J. Escarre, X. Niquille, G. Bugnon, S. Hänni, M. Bonnet-Eymard, F. Meillaud and C. Ballif, presented at the 40th IEEE PVSC, Denver, 2014.
11 S. Kim, J.-W. Chung, H. Lee, J. Park, Y. Heo and H.-M. Lee, *Sol. Energy Mater. Sol. Cells*, 2013, **119**, 26–35.
12 Applied Materials press release, 20/3/2012, http://www.appliedmaterials.com.
13 Delft University MOOC, Solar Energy, ET.3034TU, https://www.edx.org/school/delftx.
14 M. A. Green, K. Emery, Y. Hishikawa, W. Warta and E. D. Dunlop, *Progress in Photovoltaics: Research and Applications*, 2014, **22**, 701–710.
15 TEL Solar press release, 9/7/2014, http://www.solar.tel.com.
16 H. Curtins, N. Wyrsch, M. Favre and A. Shah, *Plasma Chem. Plasma Process.*, 1987, **7**, 267–273.
17 U. Kroll, J. Meier, A. Shah, S. Mikhailov and J. Weber, *J. Appl. Phys.*, 1996, **80**, 4971.
18 R. Chittick, J. Alexander and H. Sterling, *J. Electrochem. Soc.*, 1969, **116**, 77.
19 S. Usui and M. Kikuchi, *J. Non-Cryst. Solids*, 1979, **34**, 1–11.
20 A. Mahan, R. C. Kernsa and G. Devaud, *J. Electron. Mater.*, 1983, **12**, 1033–1049.

21 A. Lloret, Z. Wu, M. Theye, I. El Zawawi, J. Siefert and B. Equer, *Appl. Phys.*, 1992, **55**, 573–581.
22 R. A. Street, *Phys. Rev. Lett.*, 1982, **49**, 1187.
23 R. Street, D. Biegelsen and J. Knights, *Phys. Rev. B: Condens. Matter Mater. Phys.*, 1981, **24**, 969.
24 A. DeVos, *J. Phys. D: Appl. Phys.*, 1980, **13**, 839.
25 K. Laaziri, S. Kycia, S. Roorda, M. Chicoine, J. Robertson, J. Wang and S. Moss, *Phys. Rev. B: Condens. Matter Mater. Phys.*, 1999, **60**, 13520–13533.
26 M. Brodsky and R. Title, *Phys. Rev. Lett.*, 1969, **23**, 581–585.
27 M. Brodsky and D. Kaplan, *J. Non-Cryst. Solids*, 1979, **32**, 431–435.
28 M. Yamaguchi and K. Morigaki, *Philos. Mag. B*, 1999, **79**, 387–405.
29 J. Robertson, *J. Appl. Phys.*, 2000, **87**, 2608–2617.
30 D. L. Staebler and C. R. Wronski, *Appl. Phys. Lett.*, 1977, **31**, 292.
31 D. Staebler and C. R. Wronski, *J. Appl. Phys.*, 1980, **51**, 3262–3268.
32 D. L. Staebler, R. S. Crandall and R. Williams, *Appl. Phys. Lett.*, 1981, **39**, 733.
33 M. Stutzmann, W. Jackson and C. Tsai, *Phys. Rev. B: Condens. Matter Mater. Phys.*, 1985, **32**, 23.
34 Z. Smith and S. Wagner, *Phys. Rev. B: Condens. Matter Mater. Phys.*, 1985, **32**, 5510–5513.
35 D. Carlson, *Appl. Phys. A: Solids Surf.*, 1986, **41**, 305–309.
36 D. Redfield and R. H. Bube, *Appl. Phys. Lett.*, 1989, **54**, 1037–1039.
37 R. Street and K. Winer, *Phys. Rev. B: Condens. Matter Mater. Phys.*, 1989, **40**, 6236–6249.
38 H. M. Branz, *J. Non-Cryst. Solids*, 2000, **266**, 391–396.
39 N. Kopidakis and E. Schiff, *J. Non-Cryst. Solids*, 2000, **266**, 415–418.
40 R. Wehrspohn, M. Powell and S. Deane, *J. Appl. Phys.*, 2003, **93**, 5780–5788.
41 P. Stradins, *Sol. Energy Mater. Sol. Cells*, 2003, **78**, 349–367.
42 T. W. Herring, S. Y. Lee, D. R. McCamey, P. C. Taylor, K. Lips, J. Hu, F. Zhu, A. Madan and C. Boehme, *Phys. Rev. B: Condens. Matter Mater. Phys.*, 2009, **79**, 195205.
43 M. Fehr, A. Schnegg, B. Rech, K. Lips, O. Astakhov, F. Finger, G. Pfanner, C. Freysoldt, J. Neugebauer and R. Bittl, *Phys. Rev. B: Condens. Matter Mater. Phys.*, 2011, **84**, 245203.
44 A. H. M. Smets and M. C. M. van de Sanden, *Phys. Rev. B: Condens. Matter Mater. Phys.*, 2007, **76**, 073202.
45 J. Melskens, A. Smets, S. Eijt, H. Schut, E. Brück and M. Zeman, *J. Non-Cryst. Solids*, 2012, **358**, 2015–2018.
46 M. Fehr, A. Schnegg, B. Rech, O. Astakhov, F. Finger, R. Bittl, C. Teutloff and K. Lips, *Phys. Rev. Lett.*, 2014, **112**, 066403.
47 M. Günes and C. R. Wronski, *J. Appl. Phys.*, 1997, **81**, 3526–3536.
48 J. J. Hanak and V. Korsun, presented at the 16th IEEE PVSC, San Diego, 1982.
49 M. S. Bennett and K. Rajan, presented at the 20th IEEE PVSC, Las Vegas, 1988.
50 S. Benagli, D. Borrello, E. Vallat-Sauvain, J. Meier, U. Kroll, J. Hoetzel, J. Bailat, J. Steinhauser, M. Marmelo, G. Monteduro and L. Castens, presented at the 24th European PVSEC, Hamburg, 2009.
51 M. Stuckelberger, M. Despeisse, G. Bugnon, J.-W. Schüttauf, F.-J. Haug and C. Ballif, *J. Appl. Phys.*, 2013, **114**, 154509.
52 J. Meier, R. Flückiger, H. Keppner and A. Shah, *Appl. Phys. Lett.*, 1994, **65**, 860–862.
53 P. Torres, J. Meier, R. Flückiger, U. Kroll, J. Selvan, H. Keppner, A. Shah, S. Littelwood, I. Kelly and P. Giannoules, *Appl. Phys. Lett.*, 1996, **69**, 1373.
54 B. Strahm, A. Howling, L. Sansonnens, C. Hollenstein, U. Kroll, J. Meier, C. Ellert, L. Feitknecht and C. Ballif, *Sol. Energy Mater. Sol. Cells*, 2007, **91**, 495–502.
55 M. Van den Donker, B. Rech, F. Finger, L. Houben, W. Kessels and M. Van de Sanden, *Progress in Photovoltaics: Research and Applications*, 2007, **15**, 291–301.
56 Q. Zhang, E. Johnson, Y. Djeridane, A. Abramov and P. Roca i Cabarrocas, *Phys. Status Solidi RRL*, 2008, **2**, 154–156.
57 M. Boccard, C. Battaglia, F.-J. Haug, M. Despeisse and C. Ballif, *Appl. Phys. Lett.*, 2012, **101**, 151105.
58 H. Sai, K. Saito, N. Hozuki and M. Kondo, *Appl. Phys. Lett.*, 2013, **102**, 053509.
59 V. Smirnov, W. Böttler, A. Lambertz, H. Wang, R. Carius and F. Finger, *Phys. Status Solidi C*, 2010, **7**, 1053.
60 Y. Tawada, H. Okamoto and Y. Hamakawa, *Appl. Phys. Lett.*, 1981, **39**, 237–239.
61 T. Tiedje, *Appl. Phys. Lett.*, 1982, **40**, 627–629.
62 M. A. Green, J. Zhao, A. Wang and S. R. Wenham, *IEEE Trans. Electron Dev.*, 1999, **46**, 1940–1947.
63 M. Taguchi, A. Yano, S. Tohoda, K. Matsuyama, Y. Nakamura, T. Nishiwaki, K. Fujita and E. Maruyama, *IEEE Journal of Photovoltaics*, 2014, **4**, 96–99.
64 M. Green, *Sol. Energy Mater. Sol. Cells*, 2008, **92**, 1305–1310.
65 D. Redfield, *Appl. Phys. Lett.*, 1974, **25**, 647.
66 P. Campbell and M. Green, *J. Appl. Phys.*, 1987, **62**, 243–249.
67 E. Yablonovitch and G. D. Cody, *IEEE Trans. Electron Devices*, 1982, **29**, 300–305.
68 M. A. Green, *Sol. Energy Mater. Sol. Cells*, 2008, **92**, 1305–1310.
69 H. R. Stuart and D. G. Hall, *J. Opt. Soc. Am. A*, 1997, **14**, 3001–3008.
70 F. J. Haug, A. Naqavi and C. Ballif, *J. Appl. Phys.*, 2012, **112**, 024516.
71 P. Sheng, A. N. Bloch and R. S. Stepleman, *Appl. Phys. Lett.*, 1983, **43**, 579–581.
72 Z. Yu, A. Raman and S. Fan, *Optics Express*, 2010, **18**, A366–A380.
73 E. A. Schiff, *J. Appl. Phys.*, 2011, **110**, 104501.
74 F.-J. Haug, K. Söderström, A. Naqavi and C. Ballif, *J. Appl. Phys.*, 2011, **107**, 044504.
75 A. Cowley and S. Sze, *J. Appl. Phys.*, 1965, **36**, 3212–3220.
76 D. K. Schroder and D. L. Meier, *IEEE Trans. Electron Devices*, 1984, **31**, 637–647.
77 C. Wronski and D. Carlson, *Solid State Commun.*, 1977, **23**, 421–424.

78 C. Kothandaraman, T. Tonon, C. Huang and A. E. Delahoy, presented at the MRS Spring Meeting, San Francisco, 1991.
79 P. Delli Veneri, L. V. Mercaldo and I. Usatii, *Appl. Phys. Lett.*, 2010, **97**, 023512.
80 D. Zhou and R. Biswas, *J. Appl. Phys.*, 2008, **103**, 093102.
81 J. Krc, M. Zeman, S. Luxembourg and M. Topic, *Appl. Phys. Lett.*, 2009, **94**, 153501.
82 H. Deckman and J. Dunsmuir, *J. Vac. Sci. Technol., B: Microelectron. Nanometer Struct.–Process., Meas., Phenom.*, 1983, **1**, 1109–1112.
83 M. Zeman, R. Van Swaaij, J. W. Metselaar and R. E. I. Schropp, *J. Appl. Phys.*, 2000, **88**, 6436.
84 J. Krc, F. Smole and M. Topic, *Progress in Photovoltaics: Research and Applications*, 2003, **11**, 15–26.
85 K. Jäger, M. Fischer, R. van Swaaij and M. Zeman, *J. Appl. Phys.*, 2012, **111**, 083108.
86 M. Berginski, J. Hüpkes, A. Gordijn, W. Reetz, T. Wätjen, B. Rech and M. Wuttig, *Sol. Energy Mater. Sol. Cells*, 2008, **92**, 1037–1042.
87 A. Campa, O. Isabella, R. van Erven, P. Peeters, H. Borg, J. Krc, M. Topic and M. Zeman, *Progress in Photovoltaics: Research and Applications*, 2010, **18**, 160–167.
88 M. Zeman, O. Isabella, S. Solntsev and K. Jäger, *Sol. Energy Mater. Sol. Cells*, 2013, **119**, 94–111.
89 H. Deckman and J. Dunsmuir, *Appl. Phys. Lett.*, 1982, **41**, 377–379.
90 Z. Huang, D. Carnahan, J. Rybczynski, M. Giersig, M. Sennett, D. Wang, J. Wen, K. Kempa and Z. Ren, *Appl. Phys. Lett.*, 2003, **82**, 460–462.
91 C. M. Hsu, C. Battaglia, C. Pahud, Z. Ruan, F. J. Haug, S. Fan, C. Ballif and Y. Cui, *Adv. Energy Mater.*, 2012, **2**, 628–633.
92 M. L. Brongersma, Y. Cui and S. Fan, *Nat. Mater.*, 2014, **13**, 451–460.
93 H. Deckman, C. Roxlo and E. Yablonovitch, *Opt. Lett.*, 1983, **8**, 491–493.
94 W. J. Nam, L. Ji, V. V. Varadan and S. J. Fonash, *J. Appl. Phys.*, 2012, **111**, 123103.
95 V. E. Ferry, A. Polman and H. A. Atwater, *ACS Nano*, 2011, **5**, 10055–10064.
96 K. Söderström, G. Bugnon, R. Biron, C. Pahud, F. Meillaud, F.-J. Haug and C. Ballif, *J. Appl. Phys.*, 2012, **112**, 114503–114504.
97 A. Lambertz, V. Smirnov, T. Merdzhanova, K. Ding, S. Haas, G. Jost, R. Schropp, F. Finger and U. Rau, *Sol. Energy Mater. Sol. Cells*, 2013, **119**, 134–143.
98 F.-J. Haug, T. Söderström, O. Cubero, V. Terrazoni-Daudrix and C. Ballif, *J. Appl. Phys.*, 2009, **106**, 044502.
99 M. G. Deceglie, V. E. Ferry, A. P. Alivisatos and H. A. Atwater, *Nano Lett.*, 2012, **12**, 2894–2900.
100 K. Söderström, F. J. Haug, J. Escarré, C. Pahud, R. Biron and C. Ballif, *Sol. Energy Mater. Sol. Cells*, 2011, **95**, 3585–3591.
101 H. Iida, N. Shiba, T. Mishuku, A. Ito, H. Karasawa, M. Yamanaka and Y. Hayashi, *Electron Device Letters, IEEE*, 1982, **3**, 114–115.
102 H. Iida, N. Shiba, T. Mishuku, H. Karasawa, A. Ito, M. Yamanaka and Y. Hayashi, *Electron Device Letters, IEEE*, 1983, **4**, 157–159.
103 M. Mizuhashi, Y. Gotoh and K. Adachi, *Jpn. J. Appl. Phys., Part 1*, 1988, **27**, 2053.
104 K. Sato, Y. Gotoh, Y. Hayashi, K. Adachi and H. Nishimura, *Rep. Res. Lab., Asahi Glass Co, Ltd.*, 1990, **40**, 233–241.
105 W. W. Wenas, A. Yamada, M. Konagai and K. Takahashi, *Jpn. J. Appl. Phys., Part 1*, 1991, **30**, L441.
106 S. Faÿ, U. Kroll, C. Bucher, E. Vallat-Sauvain and A. Shah, *Sol. Energy Mater. Sol. Cells*, 2005, **86**, 385–397.
107 T. Ikeda, K. Sato, Y. Hayashi, Y. Wakayama, K. Adachi and H. Nishimura, *Sol. Energy Mater. Sol. Cells*, 1994, **34**, 379–384.
108 Y. Nasuno, M. Kondo and A. Matsuda, *Jpn. J. Appl. Phys., Part 1*, 2002, **41**, 5912.
109 H. Fujiwara, M. Kondo and A. Matsuda, *J. Appl. Phys.*, 2003, **93**, 2400–2409.
110 C. Rockstuhl, S. Fahr, K. Bittkau, T. Beckers, R. Carius, F. Haug, T. Söderström, C. Ballif and F. Lederer, *Optics Express*, 2010, **18**, A335–A341.
111 C. Rockstuhl, S. Fahr, F. Lederer, F. J. Haug, T. Soderstrom, S. Nicolay, M. Despeisse and C. Ballif, *Appl. Phys. Lett.*, 2011, **98**, 051102–051103.
112 M. Kambe, K. Masummo, N. Taneda, T. Oyama and K. Sato, presented at the 17th Int. PVSEC, Fukuoka, 2007.
113 J. Krc, B. Lipovsek, M. Bokalic, A. Campa, T. Oyama, M. Kambe, T. Matsui, H. Sai, M. Kondo and M. Topic, *Thin Solid Films*, 2010, **518**, 3054–3058.
114 H. Sakai, T. Yoshida, T. Hama and Y. Ichikawa, *Jpn. J. Appl. Phys., Part 1*, 1990, **29**, 630–635.
115 J. Hüpkes, J. Owen, E. Bunte, H. Zhu, S. Pust, J. Worbs and G. Jost, presented at the 25th European PVSEC, Valencia, 2010.
116 J. I. Owen, J. Hüpkes, E. Bunte, S. E. Pust and A. Gordijn, presented at the 25th European PVSEC, Valencia, 2010.
117 O. Kluth, B. Rech, L. Houben, S. Wieder, G. Schöpe, C. Beneking, H. Wagner, A. Löffl and H. W. Schock, *Thin Solid Films*, 1999, **351**, 247–253.
118 J. Müller, B. Rech, J. Springer and M. Vanecek, *Sol. Energy*, 2004, **77**, 917–930.
119 M. Hirasaka, K. Suzuki, K. Nakatani, M. Asano, M. Yano and H. Okaniwa, *Sol. Energy Mater.*, 1990, **20**, 99–110.
120 A. Banerjee and S. Guha, *J. Appl. Phys.*, 1991, **69**, 1030–1035.
121 R. Franken, R. Stolk, H. Li, C. van der Werf, J. Rath and R. Schropp, *J. Appl. Phys.*, 2007, **102**, 014503.
122 F.-J. Haug, T. Söderström, M. Python, V. Terrazzoni-Daudrix, X. Niquille and C. Ballif, *Sol. Energy Mater. Sol. Cells*, 2009, **93**, 884–8877.
123 T. Söderström, F. J. Haug, V. Terrazzoni-Daudrix and C. Ballif, *J. Appl. Phys.*, 2010, **107**, 014507.
124 J. Bailat, V. Terrazzoni-Daudrix, J. Guillet, F. Freitas, X. Niquille, A. Shah, C. Ballif, T. Scharf, R. Morf, A. Hansen, D. Fischer, Y. Ziegler and A. Closset, presented at the 20th European PVSEC, Barcelona, 2005.
125 H. A. Atwater and A. Polman, *Nat. Mater.*, 2010, **9**, 205–213.

126 E. Hao, G. Schatz, R. Johnson and J. Hupp, *J. Chem. Phys.*, 2002, **117**, 5963–5966.
127 K. L. Kelly, E. Coronado, L. L. Zhao and G. C. Schatz, *J. Phys. Chem. B*, 2003, **107**, 668–677.
128 H. R. Stuart and D. G. Hall, *Appl. Phys. Lett.*, 1996, **69**, 2327.
129 H. R. Stuart and D. G. Hall, *Phys. Rev. Lett.*, 1998, **80**, 5663.
130 H. R. Stuart and D. G. Hall, *Appl. Phys. Lett.*, 1998, **73**, 3815–3817.
131 S. Pillai, K. R. Catchpole, T. Trupke and M. A. Green, *J. Appl. Phys.*, 2007, **101**, 093105.
132 K. Catchpole and A. Polman, *Appl. Phys. Lett.*, 2008, **93**, 191113.
133 S. A. Maier and H. A. Atwater, *J. Appl. Phys.*, 2005, **98**, 011101.
134 F. Beck, A. Polman and K. Catchpole, *J. Appl. Phys.*, 2009, **105**, 114310.
135 R. Santbergen, R. Liang and M. Zeman, presented at the MRS Spring meeting, San Francisco, 2010.
136 A. Feltrin, T. Meguro, E. Van Assche, T. Suezaki, M. Ichikawa, T. Kuchiyama, D. Adachi, O. Inaki, K. Yoshikawa and G. Koizumi, *Sol. Energy Mater. Sol. Cells*, 2013, **119**, 219–227.
137 E. Moulin, J. Sukmanowski, M. Schulte, A. Gordijn, F. Royer and H. Stiebig, *Thin Solid Films*, 2008, **516**, 6813–6817.
138 C. Eminian, F. J. Haug, O. Cubero, X. Niquille and C. Ballif, *Progress in Photovoltaics: Research and Applications*, 2011, **19**, 260–265.
139 H. Mizuno, H. Sai, K. Matsubara and M. Kondo, *Jpn. J. Appl. Phys.*, 2012, **51**, 2302.
140 H. Tan, R. Santbergen, A. H. Smets and M. Zeman, *Nano Lett.*, 2012, **12**, 4070–4076.
141 C. Pahud, V. Savu, M. Klein, O. Vazquez-Mena, F. Haug, J. Brugger and C. Ballif, *IEEE Journal of Photovoltaics*, 2013, **3**, 22–26.
142 C. Pahud, O. Isabella, A. Naqavi, F.-J. Haug, M. Zeman, H. P. Herzig and C. Ballif, *Optics Express*, 2013, **21**, A786–A797.
143 J. Meier, S. Benagli, J. Bailat, D. Borello, J. Steinhauser, J. Hötzel, L. Castens, J. B. Orhan, Y. Djerdidane, E. Vallat-Sauvain and U. Kroll, presented at the MRS Spring Meeting, San Francisco, 2010.
144 T. Matsui, H. Sai, T. Suezaki, M. Matsumoto, K. Saito, I. Yosida and M. Kondo, presented at the 28th European PVSEC, 2013.
145 J. Yang, A. Banerjee and S. Guha, *Sol. Energy Mater. Sol. Cells*, 2003, **78**, 597–612.
146 M. J. Naughton, K. Kempa, Z. F. Ren, Y. Gao, J. Rybczynski, N. Argenti, W. Gao, Y. Wang, Y. Peng and J. R. Naughton, *Phys. Status Solidi RRL*, 2010, **4**, 181–183.
147 S. Misra, L. Yu, M. Foldyna and P. Roca i Cabarrocas, *Sol. Energy Mater. Sol. Cells*, 2013, **118**, 90–95.
148 C. Battaglia, C. M. Hsu, K. Söderström, J. Escarré, F. J. Haug, M. Charrière, M. Boccard, M. Despeisse, D. Alexander, M. Cantoni, Y. Cui and C. Ballif, *ACS Nano*, 2012, **6**, 2790–2797.
149 S.-F. Leung, L. Gu, Q. Zhang, K.-H. Tsui, J.-M. Shieh, C.-H. Shen, T.-H. Hsiao, C.-H. Hsu, L. Lu and D. Li, *Sci. Rep.*, 2014, **4**, 4243.
150 Y. Wang, K. Kempa, B. Kimball, J. B. Carlson, G. Benham, W. Z. Li, T. Kempa, J. Rybczynski, A. Herczynski and Z. F. Ren, *Appl. Phys. Lett.*, 2004, **85**, 2607.
151 T. Paudel, J. Rybczynski, Y. T. Gao, Y. C. Lan, Y. Peng, K. Kempa, M. J. Naughton and Z. F. Ren, *Phys. Status Solidi A*, 2011, **208**, 924–927.
152 W. J. Nam, L. Ji, T. L. Benanti, V. V. Varadan, S. Wagner, Q. Wang, W. Nemeth, D. Neidich and S. J. Fonash, *Appl. Phys. Lett.*, 2011, **99**, 073113.
153 M. Vanecek, O. Babchenko, A. Purkrt, J. Holovsky, N. Neykova, A. Poruba, Z. Remes, J. Meier and U. Kroll, *Appl. Phys. Lett.*, 2011, **98**, 163503.
154 J. Kim, A. J. Hong, J.-W. Nah, B. Shin, F. M. Ross and D. K. Sadana, *ACS Nano*, 2012, **6**, 265–271.
155 S. Geißendörfer, M. Vehse, T. Voss, J.-P. Richters, B. Hanke, K. von Maydell and C. Agert, *Sol. Energy Mater. Sol. Cells*, 2013, **111**, 153–159.
156 H. Sai, T. Matsui, K. Matsubara, M. Kondo and I. Yoshida, *IEEE Journal of Photovoltaics*, 2014, **4**, 1349.
157 S. Hänni, G. Bugnon, G. Parascandolo, M. Boccard, J. Escarrè, M. Despeisse, F. Meillaud and C. Ballif, *Progress in Photovoltaics: Research and Applications*, 2013, **21**, 821–826.
158 K. Yamamoto, *IEEE Trans. Electron Dev.*, 1999, **46**, 2041–2047.
159 Y. Mai, S. Klein, R. Carius, H. Stiebig, X. Geng and F. Finger, *Appl. Phys. Lett.*, 2005, **87**, 073503.
160 J. Bailat, D. Dominé, R. Schlüchter, J. Steinhauser, S. Faÿ, F. Freitas, C. Bucher, L. Feitknecht, X. Niquille, R. Tscharner, A. Shah and C. Ballif, presented at the 4th World PVSEC, Hawaii, 2006.
161 S. Faÿ, J. Steinhauser, N. Oliveira, E. Vallat-Sauvain and C. Ballif, *Thin Solid Films*, 2007, **515**, 8558–8561.
162 C. Haase and H. Stiebig, *Appl. Phys. Lett.*, 2007, **91**, 061116.
163 H. Sai and M. Kondo, *J. Appl. Phys.*, 2009, **105**, 094511.
164 Y. Nasuno, M. Kondo and A. Matsuda, *Jpn. J. Appl. Phys., Part 1*, 2001, **2**, 40.
165 M. Python, E. Vallat-Sauvain, J. Bailat, D. Dominé, L. Fesquet, A. Shah and C. Ballif, *J. Non-Cryst. Solids*, 2008, **354**, 2258–2262.
166 H. Li, R. H. Franken, R. L. Stolk, J. K. Rath and R. E. I. Schropp, *Solid State Phenom.*, 2008, **131–133**, 27–32.
167 G. Bugnon, G. Parascandolo, T. Söderström, P. Cuony, M. Despeisse, S. Hänni, J. Holovsky, F. Meillaud and C. Ballif, *Adv. Funct. Mater.*, 2012, **22**, 3665–3671.
168 P. Cuony, M. Marending, D. Alexander, M. Boccard, G. Bugnon, M. Despeisse and C. Ballif, *Appl. Phys. Lett.*, 2010, **97**, 213502–213503.
169 M. Despeisse, G. Bugnon, A. Feltrin, M. Stueckelberger, P. Cuony, F. Meillaud, A. Billet and C. Ballif, *Appl. Phys. Lett.*, 2010, **96**, 073507.
170 H. Tan, E. Psomadaki, O. Isabella, M. Fischer, P. Babal, R. Vasudevan, M. Zeman and A. H. Smets, *Appl. Phys. Lett.*, 2013, **103**, 173905.

171 E. Moulin, M. Steltenpool, M. Boccard, L. c. Garcia, G. Bugnon, M. Stuckelberger, E. Feuser, B. Niesen, R. van Erven and J.-W. Schuttauf, *IEEE Journal of Photovoltaics*, 2014, **4**, 1177.
172 M. Meier, U. Paetzold, M. Ghosh, W. Zhang, T. Merdzhanova, G. Jost, N. Sommer, S. Michard and A. Gordijn, *IEEE Journal of Photovoltaics*, 2014, **4**, 772–777.
173 M. Boccard, C. Battaglia, S. Hänni, K. Söderström, J. Escarré, S. Nicolay, F. Meillaud, M. Despeisse and C. Ballif, *Nano Lett.*, 2012, **12**, 1344–1348.
174 M. Boccard, P. Cuony, C. Battaglia, S. Hänni, S. Nicolay, L. Ding, M. Benkhaira, G. Bugnon, A. Billet, M. Charrière, K. Söderström, J. Escarré, F. Sculati-Meillaud, M. Despeisse and C. Ballif, *IEEE Journal of Photovoltaics*, 2012, **2**, 83–87.
175 M. Boccard, C. Battaglia, N. Blondiaux, R. Pugin, M. Despeisse and C. Ballif, *Sol. Energy Mater. Sol. Cells*, 2013, **119**, 12–17.
176 B. Niesen, N. Blondiaux, M. Boccard, M. Stuckelberger, R. Pugin, E. Scolan, F. Meillaud, F.-J. Haug, A. Hessler-Wyser and C. Ballif, *Nano Lett.*, 2014, **14**, 5085.
177 T. Söderström, F. J. Haug, X. Niquille, V. Terrazoni-Daudrix and C. Ballif, *Appl. Phys. Lett.*, 2009, **94**, 063501.
178 R. Biron, S. Hänni, M. Boccard, C. Pahud, G. Bugnon, L. Ding, S. Nicolay, G. Parascandolo, F. Meillaud, M. Despeisse, F. Haug and C. Ballif, *IEEE Journal of Photovoltaics*, 2013, **3**, 41–45.
179 Y. Hamakawa, H. Okamoto and Y. Nitta, *Appl. Phys. Lett.*, 1979, **35**, 187–189.
180 D. Fischer, S. Dubail, J. D. Anna Selvan, N. Pellaton Vaucher, R. Platz, C. Hof, U. Kroll, J. Meier, P. Torres, H. Keppner, N. Wyrsch, M. Goetz, A. Shah and K.-D. Ufert, presented at the 25th IEEE PVSC, Washington, D. C., 1996.
181 P. Buehlmann, J. Bailat, D. Domine, A. Billet, F. Meillaud, A. Feltrin and C. Ballif, *Appl. Phys. Lett.*, 2007, **91**, 143505.
182 J. Krc, F. Smole and M. Topic, *Sol. Energy Mater. Sol. Cells*, 2005, **86**, 537–550.
183 J. Yang, A. Banerjee and S. Guha, *Appl. Phys. Lett.*, 1997, **70**, 2975–2977.
184 S. W. Ahn, S. E. Lee and H. M. Lee, presented at the 27th European PVSEC, Frankfurt, 2012.
185 X. Xu, B. Yan, D. Beglau, Y. Li, G. DeMaggio, G. Yue, A. Banerjee, J. Yang, S. Guha, P. G. Hugger and J. D. Cohen, presented in part at the MRS Spring Meeting, San Francisco, 2008.
186 B. Yan, G. Yue, X. Xu, J. Yang and S. Guha, *Phys. Status Solidi A*, 2010, **207**, 671–677.
187 J. W. Schüttauf, G. Bugnon, M. Stuckelberger, S. Hänni, M. Boccard, M. Despeisse, F. J. Haug, F. Meillaud and C. Ballif, *IEEE Journal of Photovoltaics*, 2014, **4**, 757–762.
188 F. T. Si, D. Y. Kim, R. Santbergen, H. Tan, R. A. C. M. M. van Swaaij, A. H. M. Smets, O. Isabella and M. Zeman, *Appl. Phys. Lett.*, 2014, **105**, 063902.
189 S. Kirner, S. Nuebert, C. Schultz, O. Gabriel, B. Stannowski,B. Rech and R. Schlatman, presented at the 6th World PVSED, Kyoto, 2014.
190 I. A. Yunaz, K. Hashizume, S. Miyajima, A. Yamada and M. Konagai, *Sol. Energy Mater. Sol. Cells*, 2009, **93**, 1056–1061.
191 M. Hishida, T. Sekimoto and A. Terakawa, *Jpn. J. Appl. Phys.*, 2014, **53**, 092301.
192 T. Matsui, M. Kondo, K. Ogata, T. Ozawa and M. Isomura, *Appl. Phys. Lett.*, 2006, **89**, 142115.
193 T. Matsui, C. Chang, T. Takada, M. Isomura, H. Fujiwara and M. Kondo, *Sol. Energy Mater. Sol. Cells*, 2009, **93**, 1100–1102.
194 O. Isabella, A. H. M. Smets and M. Zeman, *Sol. Energy Mater. Sol. Cells*, 2014, **129**, 82–89.